The Astrophysical Journal, 755:110 (10pp), 2012 August 20 doi:10.1088/0004-637X/755/2/110

RADIO AND X-RAY OBSERVATIONS OF SN 2006jd: ANOTHER STRONGLY INTERACTING TYPE IIn SUPERNOVA

Poonam Chandra[1], Roger A. Chevalier[2], Nikolai Chugai[3], Claes Fransson[4], Christopher M. Irwin[2], Alicia M. Soderberg[5], Sayan Chakraborti[6], and Stefan Immler[7,8,9]
[1] Department of Physics, Royal Military College of Canada, Kingston, ON K7K 7B4, Canada; Poonam.Chandra@rmc.ca
[2] Department of Astronomy, University of Virginia, P.O. Box 400325, Charlottesville, VA 22904-4325, USA
[3] Institute of Astronomy of Russian Academy of Sciences, Pyatnitskaya Street 48, 109017 Moscow, Russia
[4] Department of Astronomy, Stockholm University, AlbaNova, SE-106 91 Stockholm, Sweden
[5] Smithsonian Astrophysical Observatory, 60 Garden Street, MS-20, Cambridge, MA 02138, USA
[6] Department of Astronomy and Astrophysics, Tata Institute of Fundamental Research, 1 Homi Bhabha Road, Colaba, Mumbai 400005, India
[7] Astrophysics Science Division, NASA Goddard Space Flight Center, Greenbelt, MD 20771, USA
[8] Center for Research and Exploration in Space Science and Technology, NASA Goddard Space Flight Center, Greenbelt, MD 20771, USA
[9] Department of Astronomy, University of Maryland, College Park, MD 20742, USA
Received 2012 April 30; accepted 2012 June 25; published 2012 August 1

ABSTRACT

We report four years of radio and X-ray monitoring of the Type IIn supernova SN 2006jd at radio wavelengths with the Very Large Array, Giant Metrewave Radio Telescope, and Expanded Very Large Array; at X-ray wavelengths with *Chandra*, *XMM-Newton*, and *Swift*-XRT. We assume that the radio and X-ray emitting particles are produced by shock interaction with a dense circumstellar medium. The radio emission shows an initial rise that can be attributed to free–free absorption by cool gas mixed into the nonthermal emitting region; external free–free absorption is disfavored because of the shape of the rising light curves and the low gas column density inferred along the line of sight to the emission region. The X-ray luminosity implies a preshock circumstellar density $\sim 10^6$ cm^{-3} at a radius $r \sim 2 \times 10^{16}$ cm, but the column density inferred from the photoabsorption of X-rays along the line of sight suggests a significantly lower density. The implication may be an asymmetry in the interaction. The X-ray spectrum shows Fe line emission at 6.9 keV that is stronger than is expected for the conditions in the X-ray emitting gas. We suggest that cool gas mixed into the hot gas plays a role in the line emission. Our radio and X-ray data both suggest the density profile is flatter than r^{-2} because of the slow evolution of the unabsorbed emission.

Key words: circumstellar matter – hydrodynamics – radio continuum: general – stars: mass-loss – supernovae: general – supernovae: individual (SN 2006jd)

Online-only material: color figures

1. INTRODUCTION

Type IIn supernovae (SNe IIn) are a subclass of supernovae (SNe) that show characteristic narrow emission lines of hydrogen and helium in their spectra (Schlegel 1990; Filippenko 1997). These SNe are thought to have dense circumstellar media (CSM), and their high Hα and bolometric luminosities can be explained by the shock interaction of SN ejecta with the dense CSM (Chugai 1990; Chugai & Danziger 1994). Observed late excesses of infrared (IR) radiation are suggestive of dense circumstellar dust (Gerardy et al. 2002; Fox et al. 2011). Generally SNe IIn show significant heterogeneity in terms of their emission line profiles and luminosities, and apparent mass-loss history. For example, SN 1998S demonstrates a connection between the Type IIL and the Type IIn class: the light curve and spectra resemble those of the bright Type IIL SN 1979C and yet the Hα line shows Type IIn characteristics (Fassia et al. 2001). SN 1994W faded within 130 days, whereas SN 1988Z remained bright for a decade after the explosion. The Type IIn SN 2005gl has a possible luminous blue variable star identified as its progenitor (Gal-Yam & Leonard 2009). SNe IIn are relatively rare, comprising $\lesssim$10% of all core-collapse SNe (Smartt 2009; Li et al. 2011).

Dense circumstellar interaction in SNe IIn is expected to produce optical, radio, and X-ray emission. Radio emission in SNe IIn is expected to be synchrotron emission, initially absorbed mainly by free–free absorption, while X-ray emission is likely to have a thermal origin (Chevalier 1982). Because of the high density of the CSM, the emission due to the CSM interaction is expected to be high. SNe IIn are relatively X-ray luminous, exceeding 10^{40} erg s^{-1} in some cases, e.g., SN 1988Z (Fabian & Terlevich 1996; Schlegel & Petre 2006) and SN 1986J (Bregman & Pildis 1992, 1994; Temple et al. 2005). However, SNe IIn have been elusive at radio wavelengths. So far, only 10 SNe IIn have been detected in the radio. van Dyk et al. (1996) carried out a search for radio emission from 10 SNe IIn and did not detect any.

SN 2006jd was discovered on 2006 October 12, with an apparent magnitude of 17.2, in the galaxy UGC 4179 at a redshift of $z = 0.0186$ (Prasad & Li 2006). The initial spectrum of SN 2006jd showed features of a Type IIb SN, similar to SN 1993J (Blondin et al. 2006). However, based on Keck spectra at late epochs, it was reclassified as a Type IIn SN (A. Filippenko, 2006, private communication). On the basis of a spectrum on 2006 October 17.51 UT, we assume its explosion date to be 2006 October 06.5 UT (Blondin et al. 2006). It is located at R.A. = $08^{\rm h}02^{\rm m}07\overset{\rm s}{.}43$, decl. = $+00^\circ48'31\overset{''}{.}5$ (equinox 2000.0), which is $22''$ east and $1\overset{''}{.}3$ south of the nucleus of UGC 4179. Immler et al. (2007) detected X-ray emission from SN 2006jd on 2007 November 16 with the *Swift* X-ray Telescope (XRT) in a 2.3 ks exposure. The net count rate was $(6.3 \pm 2.0) \times 10^{-3}$ counts s^{-1}. For an adopted plasma model with a temperature of 10 keV and a Galactic column density of 4.5×10^{20} cm^{-2}, they estimated an unabsorbed luminosity of $(2.5 \pm 0.8) \times 10^{41}$ erg s^{-1}, placing it in the category of highly X-ray luminous SNe IIn. Radio emission was detected from the SN on 2007 November 21.28 UT in the

5 GHz band, on 2007 November 26.36 UT in the 8.5 GHz band, and on 2007 November 26.38 UT in the 22.5 GHz band (Chandra & Soderberg 2007).

In this paper, we report four years of radio and X-ray monitoring of SN 2006jd and its implications for the CSM density and the mass-loss rate of the progenitor star. In Section 2, we describe the radio and X-ray observations, and their analysis in Section 3. We discuss the main results and present conclusions in Section 4.

2. OBSERVATIONS

2.1. Radio Observations

Radio observations of SN 2006jd started on 2007 November 21.28 UT with the Very Large Array[10] (VLA). We observed the SN in the 22.5 GHz (*K* band), 8.5 GHz (*X*), 5 GHz (*C*), and 1.4 GHz (*L*) bands at various epochs, along with a 44 GHz band observation at one epoch. For *C* and *X* bands, the data were taken in the interferometric mode for an average of 30 minutes (including calibrator time), whereas for *L* and *K* bands the data were collected for 1 hr. The total bandwidth used was 50 MHz. 3C48 was used as the flux calibrator and J0739+016 was used for the phase calibration. The VLA observed SN 2006jd over the period 2007 November 21.28 to 2009 August 7.75. From 2010 June onward, the observations were made using the Expanded VLA (EVLA). For EVLA observations, 3C48 and J0739+016 were also used as bandpass calibrators. The data were analyzed using standard AIPS routines.

We also observed SN 2006jd with the Giant Metrewave Radio Telescope (GMRT) on three occasions between 2009 October to 2010 April in the 1.3 GHz and 0.61 GHz bands. We detected the SN in the 1.3 GHz band at both occasions, whereas observations at 0.61 GHz resulted in upper limits. For GMRT observations, 3C48 and 3C147 were used as flux calibrators and J0739+016 as a phase calibrator. All these calibrators were also used for bandpass calibration. In the GMRT observations, the observing time on SN 2006jd was approximately 3 hr in each observation and a bandwidth of 32 MHz was used. AIPS was used to analyze the GMRT data as well.

Details of all the radio observations are listed in Table 1. We show the radio light curves of SN 2006jd at various frequencies in Figure 1 and radio spectra at various epochs in Figure 2.

2.2. X-Ray Observations

SN 2006jd was observed with the *Swift* onboard XRT at various epochs between 2007 November and 2011 March. In addition, we also observed it once with the *Chandra* and once with the *XMM-Newton* X-ray observatories.

We carried out the *XMM-Newton* observations under our proposal 55085 starting 2009 April 7 at 4:36:46 UT and continuing until 16:50:06 UT on 2009 April 7. The observations were carried out with the EPIC-PN and EPIC-MOS cameras in full frame with thin filter mode. The exposures for the EPIC-MOS1 and EPIC-MOS2 were 42.667 ks and 42.672 ks, respectively, and for the EPIC-PN, the exposure time was 41.032 ks. The *XMM-Newton* onboard Optical Monitor also observed the SN in UVW1, UVM2, and UVW2 filters for 5, 10, and 14.3 ks, respectively.

[10] The Very Large Array is operated by the National Radio Astronomy Observatory, a facility of the National Science Foundation operated under cooperative agreement by Associated Universities, Inc.

Table 1
Radio Observations of SN 2006jd

Tel.	Date of Observation	Days since Explosion	Freq. (GHz)	Flux Density (uJy)	rms (uJy)
VLA	2007 Nov 21.28	404.74	8.46	238	38
VLA	2007 Nov 26.38	409.84	4.86	170	38
VLA	2007 Nov 26.38	409.84	22.46	324	54
VLA	2008 Mar 07.23	511.69	8.46	305	46
VLA	2008 Mar 07.24	511.70	4.86	232	37
VLA	2008 Mar 07.26	511.72	22.46	428	41
VLA	2008 Mar 07.30	511.76	1.43	<222	74
VLA	2008 May 02.88	568.34	43.31	<1680	560
VLA	2008 May 08.15	573.61	8.46	525	50
VLA	2008 May 08.17	573.63	4.86	480	54
VLA	2008 May 10.18	575.64	1.43	<291	97
VLA	2008 May 16.00	581.46	8.46	509	42
VLA	2008 May 16.94	582.40	1.43	209	63
VLA	2008 May 25.96	591.42	22.46	683	229
VLA	2008 Dec 15.38	794.84	8.46	1024	42
VLA	2008 Dec 15.40	794.86	4.86	1035	51
VLA	2008 Dec 15.41	794.87	1.43	250	65
VLA	2008 Dec 15.45	794.91	22.46	624	90
VLA	2009 Feb 03.16	844.62	8.46	1033	23
VLA	2009 Feb 03.22	844.68	4.86	1192	26
VLA	2009 Feb 03.28	844.74	1.43	247	43
VLA	2009 Feb 03.34	844.80	22.46	665	43
VLA	2009 Apr 02.02	902.48	8.46	1069	71
VLA	2009 Apr 02.04	902.50	4.86	1178	55
VLA	2009 Apr 02.06	902.52	1.43	552	47
VLA	2009 Apr 02.10	902.56	22.46	390	55
VLA	2009 Aug 07.67	1030.13	8.46	770	50
VLA	2009 Aug 07.69	1030.15	4.86	1608	52
VLA	2009 Aug 07.71	1030.17	1.43	743	123
VLA	2009 Aug 07.75	1030.21	22.46	<645	215
GMRT	2009 Oct 21.00	1104.46	1.28	730	124
GMRT	2010 Feb 09.65	1216.11	1.28	674	79
GMRT	2010 Apr 24.52	1289.98	0.61	<441	147
EVLA	2010 Jun 06.91	1333.28	4.96	2216	54
EVLA	2010 Jul 25.67	1382.13	8.46	918	37
EVLA	2011 Jul 09.72	1731.18	4.50	1659	43
EVLA	2011 Jul 09.72	1731.18	7.92	1045	33
EVLA	2011 Jul 30.65	1752.11	22.46	<405	135
EVLA	2011 Jul 31.72	1753.18	1.39	1642	96
EVLA	2012 Apr 01.96	1998.42	4.50	1385	350
EVLA	2012 Apr 01.96	1998.42	7.90	966	25
EVLA	2012 Apr 03.02	1999.48	1.39	1564	208
EVLA	2012 Apr 07.99	2004.45	22.46	468	66

Note. Here the upper limits are 3σ upper limits.

We used the EPIC-PN observation to carry out a detailed spectroscopic analysis. The *XMM-Newton* software SAS was used to extract the spectrum. A total of 1963 counts were obtained in the 0.2–10 keV range, resulting in a net count rate of $(6.19 \pm 0.17) \times 10^{-2}$ counts s^{-1}. The NASA HEASARC software HEAsoft[11] was used to do the spectral analysis.

We also observed SN 2006jd with *Chandra* under our proposal 10500688. The observations were carried out using ACIS-S with grating NONE in the VFAINT mode. The observations started on 2009 September 14 at 00:03:21 UT for a total exposure of 37.24 ks. A total of 888 counts were obtained in the 0.2–10 keV range with a count rate of $(2.38 \pm 0.08) \times 10^{-2}$ counts s^{-1}. We extracted the spectrum using CIAO software and used HEAsoft to analyze the spectrum.

[11] http://heasarc.gsfc.nasa.gov/docs/software/lheasoft/

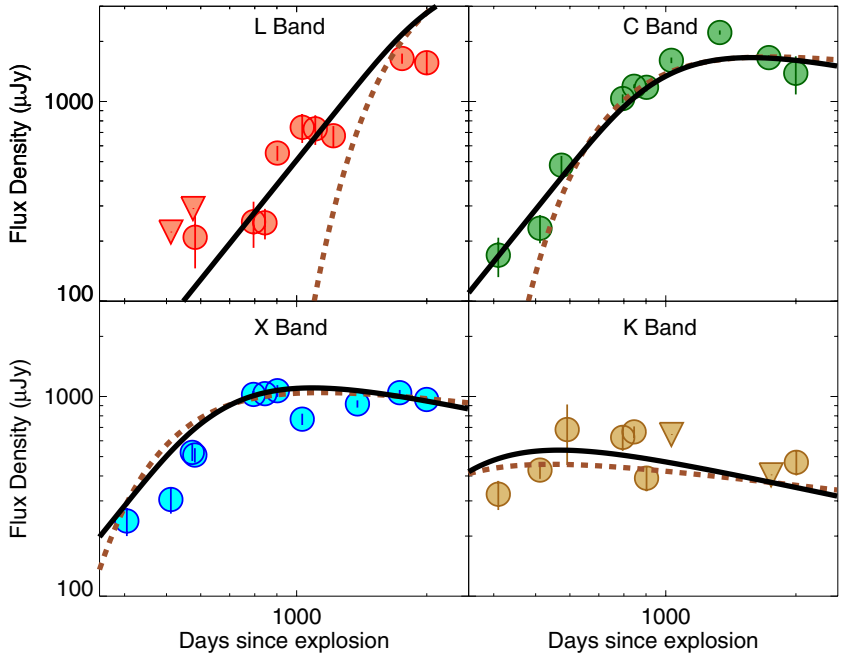

Figure 1. Radio light curves of SN 2006 in the 1.4 GHz (L), 5 GHz (C), 8.5 GHz (X), and 22.5 GHz (K) bands. The radio emission in the L band is still rising and the K-band emission appears to be in the optically thin phase at late times. The radio emission is making a transition from optically thick to thin in the X and C bands. Here dashed lines show the best-fit external absorption model for $s = 1.77$. Black solid lines are the best-fit internal absorption model.

(A color version of this figure is available in the online journal.)

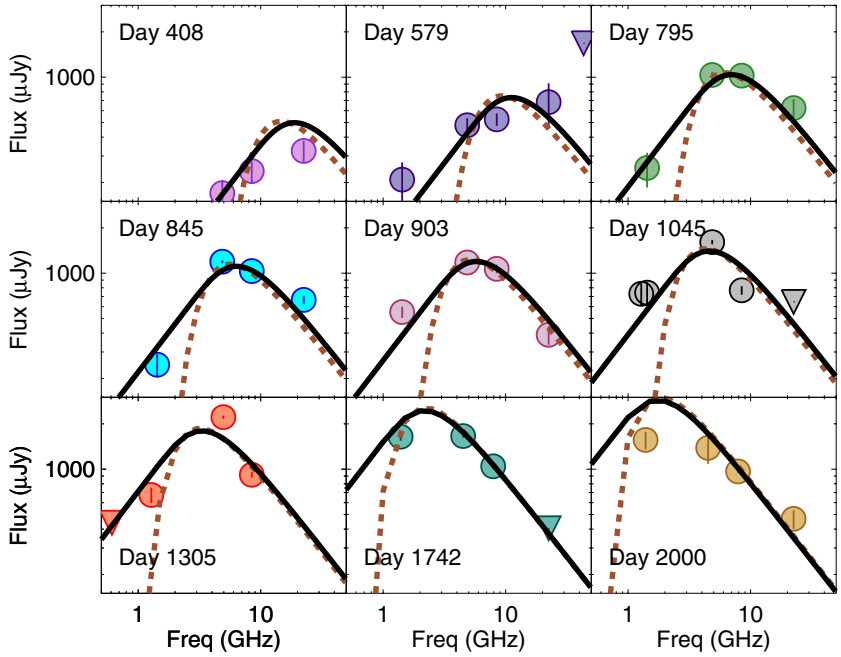

Figure 2. Radio spectra of SN 2006jd at nine epochs. Even though the spectral evolution is slow, a transition from optically thick to an optically thin is clearly seen in the progression of the spectra from early to late epochs. Dashed lines show the best-fit external absorption model for $s = 1.77$. Black solid lines are the best-fit internal absorption model.

(A color version of this figure is available in the online journal.)

Swift-XRT observed SN 2006jd on 18 occasions between 2007 November and 2011 March. All the *Swift* observations were for exposures less than 10 ks. The observations were carried out in the photon-counting mode. To extract the counts from the *Swift* observations, we combined the near-simultaneous observations and estimated the count rates using XIMAGE and SOSTA of the HEAsoft package.

Table 2 gives all the X-ray observations used in this paper. Table 3 lists the *Swift* observations which were combined to obtain the count rates. The table gives the best estimates of count rates extracted within the 0.2–10 keV range. We also obtained the best-fit positions of SN 2006jd in various *Swift* observations and estimated the position error in arcseconds from that of the actual SN position.

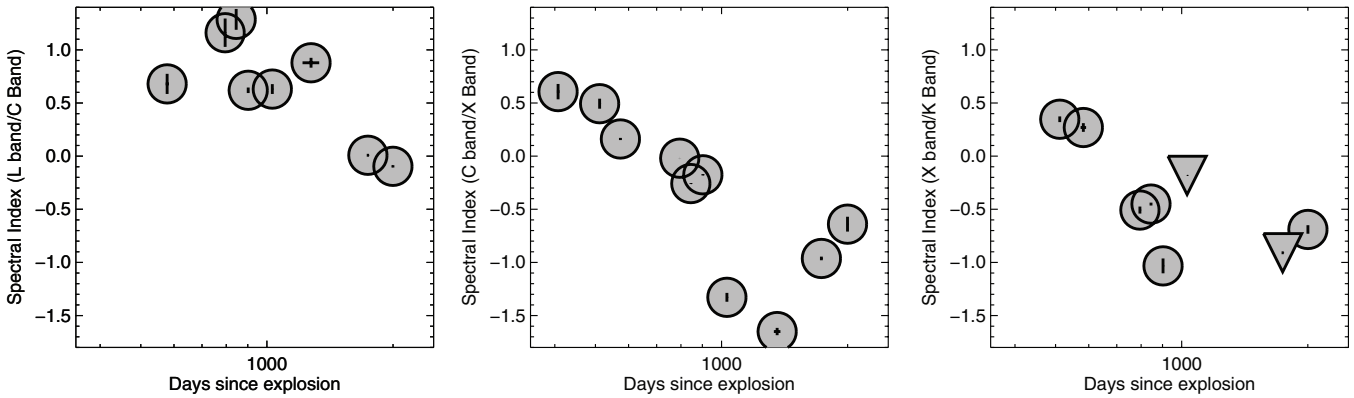

Figure 3. Spectral index (α) evolution for SN 2006jd between various radio frequencies. The evolution is from positive index toward negative, typical in core-collapse SNe.

Table 2
Details of X-Ray Observations of SN 2006jd

Date of Observation	Mission	Inst.	ObsID	Exposure (ksI)
2007 Nov 16.73	*Swift*	XRT	00031016001	2.11
2007 Nov 21.49	*Swift*	XRT	00031016002	2.92
2007 Nov 22.03	*Swift*	XRT	00031016003	1.61
2007 Nov 22.84	*Swift*	XRT	00031016004	3.06
2007 Dec 18.01	*Swift*	XRT	00031016006	9.55
2008 Jan 15.32	*Swift*	XRT	00031016007	9.26
2008 Feb 20.18	*Swift*	XRT	00031016008	3.93
2008 Feb 21.32	*Swift*	XRT	00031016009	6.06
2008 Sep 09.02	*Swift*	XRT	00031016010	1.76
2008 Sep 10.82	*Swift*	XRT	00031016011	2.49
2008 Sep 11.02	*Swift*	XRT	00031016012	7.36
2009 Apr 07.20	*XMM*	EPIC-PN	0550850101	42.92
2009 Sep 10.12	*Swift*	XRT	00031016013	9.79
2009 Sep 14.00	*Chandra*	ACIS-S	10127	37.24
2011 Mar 08.32	*Swift*	XRT	00037767006	1.06
2011 Mar 08.38	*Swift*	XRT	00037767004	0.99
2011 Mar 08.46	*Swift*	XRT	00037767005	1.01
2011 Mar 09.32	*Swift*	XRT	00037767007	3.72
2011 Mar 10.81	*Swift*	XRT	00037767008	3.12
2011 Mar 12.41	*Swift*	XRT	00037767009	2.35

3. DATA ANALYSIS AND INTERPRETATION

3.1. Radio Data Analysis and Interpretation

SN 2006jd remained bright in all the radio bands over the four-year span of observations, except for two early upper limits in L band and occasional upper limits in the K band at later epochs. Figure 1 shows the light curve of the SN in L, C, X, and K bands. The SN was in the optically thick regime in the L band, whereas it reached the optically thin regime in the K band. In the X and the C bands, the SN was close to the peak of the light curve, indicating a transition from the optically thick to the optically thin phase. The near-simultaneous spectra are plotted from day 408 to day 2000 (see Figure 2). The radio observations of SN 2006jd show an evolution from a somewhat positive spectral index to a negative index (see Figure 3). This type of evolution is commonly observed in radio SNe (Weiler et al. 2002) and is attributed to the transition from optically thick to optically thin radiation. The transition can be clearly seen by comparing progressive spectra from the earlier to the late epochs, where the peak is shifting from the higher frequencies to lower frequencies with time.

The primary mechanisms for absorption in the radio emission are free–free absorption (FFA) by the circumstellar material and synchrotron self-absorption (SSA; Chevalier 1982; Chevalier & Fransson 2003). The relevance of SSA can be determined from the peak radio luminosity and the time of peak, which can be related to the velocity of the radio emitting region if SSA dominates (Chevalier 1998; Chevalier & Fransson 2003). For SN 2006jd, we find a velocity of 2000–3000 km s^{-1} assuming the SSA absorption mechanism, which is smaller than expected in a typical SN and also than the velocities deduced from the X-ray emission for SN 2006jd (Section 3.3). We thus conclude that SSA cannot account for sufficient absorption and FFA is likely to dominate, although more complicated models (e.g., CSM clumpiness or global asymmetry) might relax constraints on the SSA mechanism imposed by the expansion velocity.

We concentrate on FFA models, allowing for the possibility of a relatively flat density profile in SN 2006jd. At the high mass-loss rates characteristic of SNe IIn, it is plausible that the density profile is not that of a steady wind. We fit the external FFA model (Chevalier 1982; Weiler et al. 2002) to the SN 2006jd data with a generalized CSM power-law density dependence $\rho \propto r^{-s}$ (Fransson et al. 1996):

$$F(\nu, t) = K_1 \left(\frac{\nu}{5\,\mathrm{GHz}}\right)^{\alpha} \left(\frac{t}{1000\,\mathrm{days}}\right)^{\beta} \exp(-\tau_{\mathrm{FFA}}),$$
$$\tau_{\mathrm{FFA}} = K_2 \left(\frac{\nu}{5\,\mathrm{GHz}}\right)^{-2.1} \left(\frac{t}{1000\,\mathrm{days}}\right)^{\delta}, \quad (1)$$

where α is the optically thin frequency spectral index, which relates to the electron energy index γ ($N(E) \propto E^{-\gamma}$) as $\gamma = 1 - 2\alpha$. To determine the value of α, we choose the average of spectral indices between K and X bands and X and C bands in Figure 3 after it has become optically thin. This value is $\alpha = -1.04 \pm 0.05$. Thus, we fix $\alpha = -1.04$ ($\gamma = 3.08$) in the radio absorption models. The parameter δ is related to the expansion parameter m ($R \propto t^m$, where R is the shock radius) and the CSM density power-law index s (in $\rho \propto r^{-s}$) as $\delta = m(1 - 2s)$. The assumption that the energy density in the particles and the fields is proportional to the postshock energy density leads to $\beta = 3m - (3 - \alpha)(ms + 2 - 2m)/2$. Here, K_1 is the radio flux density normalization parameter and K_2 is the external FFA optical depth normalization parameter. Using these parameters, we fit the SN 2006jd radio data to Equation (1). We first fit the data for standard $s = 2$ model in Equation (1), which gives a very poor fit (Table 4). The best-fit δ here is $\delta = 3.46 \pm 0.02$ implying $m = 1.15$. Allowing

Table 3
Count Rates Obtained from *Swift*-XRT Observations

ObsID	Exposure (s)	R.A. (J2000)	Decl. (J2000)	Error (″)	Count Rate (counts s^{-1})
0031016001-004	9695.659	08:02:07.2	+00:48:31.9	3.47	$(6.816 \pm 1.100) \times 10^{-03}$
0031016006	9547.694	08:02:07.1	+00:48:34.0	5.55	$(6.464 \pm 1.100) \times 10^{-03}$
0031016007	9261.903	08:02:07.3	+00:48:33.7	2.94	$(7.421 \pm 1.200) \times 10^{-03}$
0031016008-009	9991.502	08:02:07.5	+00:48.33.3	2.00	$(6.011 \pm 1.000) \times 10^{-03}$
00310160010-012	11621.214	08:02:07.1	+00:48:28.9	5.59	$(8.094 \pm 1.100) \times 10^{-03}$
0031016013	9750.140	08:02:07.4	+00:48:29.5	2.05	$(4.549 \pm 0.910) \times 10^{-03}$
0037767004-009	12151.953	08:02:07.5	+00:48:30.4	1.52	$(5.608 \pm 0.910) \times 10^{-03}$

Table 4
Model Fits to SN 2006jd Radio Data (assuming $\alpha = -1.04$)

Model	χ^2/ν	Param-1	Param-2	Param-3	Param-4	Param-5
External FFA ($s = 2$)	2.41	$K_1 = (2.27 \pm 0.03) \times 10^3$	$K_2 = 0.46 \pm 0.01$	$\delta = 3.46 \pm 0.02$	...	...
External FFA (flatter s)	2.11	$K_1 = (2.05 \pm 0.03) \times 10^3$	$K_2 = 0.40 \pm 0.01$	$s = 1.77 \pm 0.02$	$m = 1.09 \pm 0.01$	...
Internal FFA	1.26	$K_1 = (2.30 \pm 0.04) \times 10^3$	$K_3 = 1.20 \pm 0.04$	$\beta = 0.46 \pm 0.04$	$\delta' = 3.15 \pm 0.07$	...
Internal+External FFA	1.30	$K_1 = (2.31 \pm 0.04) \times 10^3$	$K_2 = 0.002 \pm 0.003$	$K_3 = 1.22 \pm 0.05$	$\delta = 3.58 \pm 0.04$	$\delta' = 3.16 \pm 0.07$

for a flatter density profile, our data are best fit with a value $m = 1.09$ and $s = 1.77$ (Table 4). Dashed lines in Figures 1 and 2 show the external FFA fit to the radio data for SN 2006jd with $s = 1.77$. The fit to the data is not perfect and the value $m > 1$ is a problem because the model for the emission requires that $m \leqslant 1$ (Chevalier 1982). We explored models with $m < 1$, but found that they did not give an acceptable fit to the data.

A property of the external absorption model is that there is an initial exponential ($e^{-\tau}$) rise in the flux. The data appear to give more of a power-law rise, which is also observed in other SNe IIn where the rise of the radio flux was followed: SN 1986J (Weiler et al. 1990) and SN 1988Z (van Dyk et al. 1993; Williams et al. 2002). Weiler et al. (1990) proposed a model in which thermal absorbing gas is mixed into the synchrotron emitting gas, so that the flux takes the form

$$F(\nu, t) = K_1 \left(\frac{\nu}{5\,\mathrm{GHz}}\right)^{\alpha} \left(\frac{t}{1000\,\mathrm{days}}\right)^{\beta} \left(\frac{1 - \exp(-\tau_{\mathrm{intFFA}})}{\tau_{\mathrm{intFFA}}}\right),$$
$$\tau_{\mathrm{intFFA}} = K_3 \left(\frac{\nu}{5\,\mathrm{GHz}}\right)^{-2.1} \left(\frac{t}{1000\,\mathrm{days}}\right)^{\delta'}, \quad (2)$$

where again we allow $s \neq 2$, so that β can be expressed as before. Weiler et al. (1990) assume that the internal absorbing gas is homologously expanding with density $n \propto R^{-3} \propto t^{-3m}$. Then $\tau_{\mathrm{intFFA}} \propto n^2 R \propto t^{-5m}$, or $\delta' = -5m$. We did not make that assumption in our fits because there are other possibilities for the evolution of the density. The internal absorbing gas is likely to be in pressure equilibrium with the surrounding hot gas and photoionized by the energetic radiation field. If the gas temperature evolves slowly, we have $n \propto p \propto R^{2-s} t^{-2}$ where p is the pressure, so that $\delta' = -4 + m(5 - 2s)$. In our fits, we allow δ' to be a free parameter.

We considered models that allowed for external as well as internal FFA. However, we found that external absorption played a negligible role in the best-fit case, while the internal absorption by itself provided an excellent fit. The fits are shown in Figures 1 and 2 and the model parameters are shown in Table 4. A notable feature of the fits is the small magnitude of β, which is associated with the slow evolution in the optically thin regime that can be seen in the late light curve evolution (Figure 1). Taking $s = 2$ for the given β implies $m = 1.19$, which is not consistent with the hydrodynamic model. However, a density profile with $s = 1.5$ gives $m = 0.9$, which is a plausible value. In this model, the value of δ' is between the values found in the two density evolution models described above.

It can be seen from Equation (2) that in the optically thick limit $F(\nu) \propto \nu^{2.1+\alpha}$. The value of α is determined by the late optically thin evolution. The fact that the optically thick spectrum is approximately reproduced (Figure 2) provides support for the internal FFA model.

The preferred model has an optical depth of unity at 5 GHz at an age of 1000 days. Assuming that the absorbing gas is in pressure equilibrium with the X-ray emitting gas and that it has a relatively low temperature (10^4–10^5 K), it is possible to estimate the mass of the gas. We determined the X-ray emitting gas has a temperature $T > 20$ keV. If we take $T \approx 60$ keV, corresponding to a shock velocity $v_{\mathrm{sh}} = 6700$ km s^{-1}, the density of the X-ray emitting gas is 6×10^6 cm^{-3} at 1000 days (Section 3.3). In pressure equilibrium, the density of cool gas is then $n_c \approx 3.6 \times 10^{11}\, T_4^{-1}$ cm^{-3}, where T_4 is the temperature in units of 10^4 K. The optical depth is $\tau = \kappa_\nu \ell$, where ℓ is the path length through the cool gas and $\kappa_\nu = 3.6 \times 10^{-27} n^2 T_4^{-3/2}$ cm^{-1} is the FFA coefficient. The absorbing mass is $M_a \approx 4\pi R_c^2 \bar{m} n_c \ell$, where R_c is the typical radius of the absorbing gas, $\bar{m}$ is the mean particle weight, and the optical depth constraint can be used to determine $n_c \ell$. The result is $M_a \approx 2 \times 10^{-8}\, T_4^{5/2} M_\odot$, showing that a modest amount of cool gas mixed into the emitting region can give rise to the needed absorption. The source of the cool gas is likely to radiative cooling of dense gas in the shocked region.

The models presented here assume a constant spectral index for the radiating electrons. Physical effects, such as Coulomb losses at low energies and synchrotron losses at high energies, can affect the particle spectrum (Fransson & Björnsson 1998). Estimates of these effects indicate that they might be significant, but a complete discussion is beyond the aims of this paper.

3.2. X-Ray Data Analysis

3.2.1. XMM-Newton

The X-ray data were best fit with a thermal plasma model at a temperature above 10 keV, i.e., in a range where the

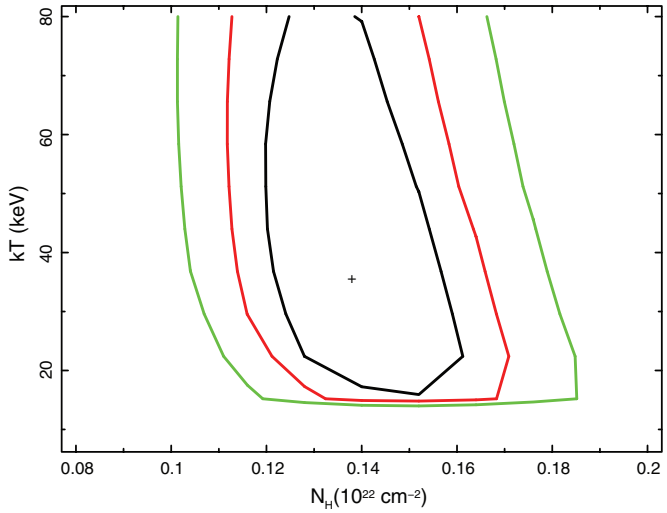

Figure 4. Confidence contours of column density vs. the X-ray emitting plasma temperature. The column density is well constrained whereas the temperature is not constrained at the higher end.

(A color version of this figure is available in the online journal.)

0.2–10 keV spectral shape is not sensitive to temperature. The spectrum also indicates a column density of 1.3×10^{21} cm^{-2}, which is significantly larger than the Galactic absorption column density of 4.5×10^{20} cm^{-2} in that direction. To determine the significance of the best-fit temperature and the column density, we plot 68%, 90%, and 99% confidence contours of column density $N_{\rm H}$ versus the plasma temperature kT. While the column density is a well-constrained parameter, the temperature is unconstrained at the upper end (see Figure 4). To better constrain the temperature, we lowered the temperature until the χ^2 became significantly worse and the fit was visibly bad. This temperature is 20 keV. We thus assign 20 keV as the lower limit to the plasma temperature.

We have a clear detection of a line between 6.5 and 7.0 keV. The line is best fit at energy 6.76 keV, which, after redshift correction, corresponds to an energy of 6.89 keV. We associate this with the 6.9 keV Fe line, which is due to Fe XXVI. There is also an evidence of a possible 8.1 keV line, which can be attributed to Ni XXVIII. To determine the significance of these lines, we plot confidence contours of their energies versus the respective strengths (Figure 5). The Fe 6.9 keV line is detected at a high significance level, whereas the 8.1 keV line is significant only at the 68% level.

Now we attempt to fit the whole spectrum. Since the temperature is very high, we explore the possibility of nonthermal emission. The best-fit power-law photon index of $\Gamma = 1.22 \pm 0.09$ is so flat that we consider this model unlikely. If we fit the Mekal model with a solar abundance, it does not reproduce the Fe 6.9 keV line. However, a Mekal model with five times the solar abundance does fit the spectrum well and reproduces the iron line at the correct energy but with a narrower width. To look for the possibility of nonequilibrium ionization (NEI), we also fit the XSPEC NEI model to our data. The fit is quite good and it reproduces the iron line at the correct energy. The best-fit ionization timescale in the NEI model is $\tau = 6.28 \times 10^{11}$ s cm^{-3}. Since $\tau = nt$ (n is the number density and t is the age) and the *XMM* spectrum was taken when the SN age was 908 days (or 7.84×10^7 s), this implies a number density of $n = 7.7 \times 10^3$ cm^{-3}. This seems low and we will discuss the physical viability of the NEI model in Section 4. Finally, we fit the thermal bremsstrahlung model with one Gaussian line fit as well as two Gaussians. The fit is not improved by adding the Gaussian at 8.1 keV. Best fits are given in Table 5 and our best-fit spectra are in Figure 6. We chose the bremsstrahlung model along with the Gaussian to be the best-fit representation to our data. The equivalent width of the Fe line is 1.4 keV and the flux in the iron line is about 10% of the total continuum flux in the 0.2–10 keV spectrum.

3.2.2. Chandra-ACIS

The *Chandra* spectrum is best fit with a high-temperature thermal plasma and a column density of 1.6×10^{21} cm^{-2}, which agree with our fits to the *XMM-Newton* spectrum very well. Even though the *Chandra* spectrum is not as detailed as that of the *XMM-Newton*, we clearly detect the 6.9 keV Fe line, though the 8.1 keV line possibly seen in the *XMM-Newton* spectrum is not present. As in the *XMM-Newton* spectrum, the temperature is not well constrained on the upper end, whereas the column density is well constrained. The iron 6.9 keV line is also well constrained at the 90% confidence level.

Because of the high temperature, we again look for the possibility of nonthermal emission; a fit yields a power-law photon index of $\Gamma = 1.31 \pm 0.14$, which again is implausibly flat. The NEI model correctly reproduced the Fe 6.9 keV line but again indicates a low density ($n = 4 \times 10^3$ cm^{-3}). The Mekal model with five times solar abundance does reproduce the Fe 6.9 keV line. We fit a bremsstrahlung model with a Gaussian at 6.9 keV. The details of the *Chandra* best-fit spectrum are in Table 6. Figure 6 shows the *XMM-Newton* and *Chandra* spectra of SN 2006jd.

3.2.3. Swift-XRT

The exposures in the *Swift* observations were not large and carrying out an independent spectroscopic analysis was not possible with the small number of counts obtained. Thus, we converted the count rates to 0.2–10 keV fluxes using a thermal plasma model with a temperature of 60 keV and column density of 1.3×10^{21} cm^{-2}.

Table 7 gives the unabsorbed fluxes at the various epochs of observation used in this paper. We also convert the X-ray fluxes to luminosities using a UGC 4179 distance of 79 Mpc. Figure 7 shows the 0.2–10 keV X-ray light curve for SN 2006jd. The flux evolution is slow and is best fit with a power-law index of $t^{-0.24 \pm 0.12}$.

3.3. X-Ray Interpretation

The *XMM-Newton* and *Chandra* X-ray spectra can be fit by either an optically thin thermal spectrum, which leads to an electron temperature $T_e \gtrsim 20$ keV, or a nonthermal spectrum with photon index $\Gamma \approx 1.2$. In the nonthermal interpretation, flux $\propto \nu^{-0.2}$ (as $\alpha = 1 - \Gamma$) would be a surprisingly hard spectrum for either synchrotron or inverse Compton emission. In the case of synchrotron radiation, one can show that for a plausible emitting volume (determined by the SN shock velocity), the radiating particle would rapidly lose energy to synchrotron radiation, tending to steepen the spectrum, and making the flat spectrum more unlikely. Thus, we discard the nonthermal origin of X-rays and proceed with the interpretation for the thermal origin of the X-ray spectrum.

In the thermal interpretation, the temperature T is assumed to be produced by shock heating, with the shock velocity $v_{\rm sh} = [16kT/(3\,\mu m_p)]^{1/2} = 6700(kT/60\,{\rm keV})^{1/2}$ km s^{-1}, where k is

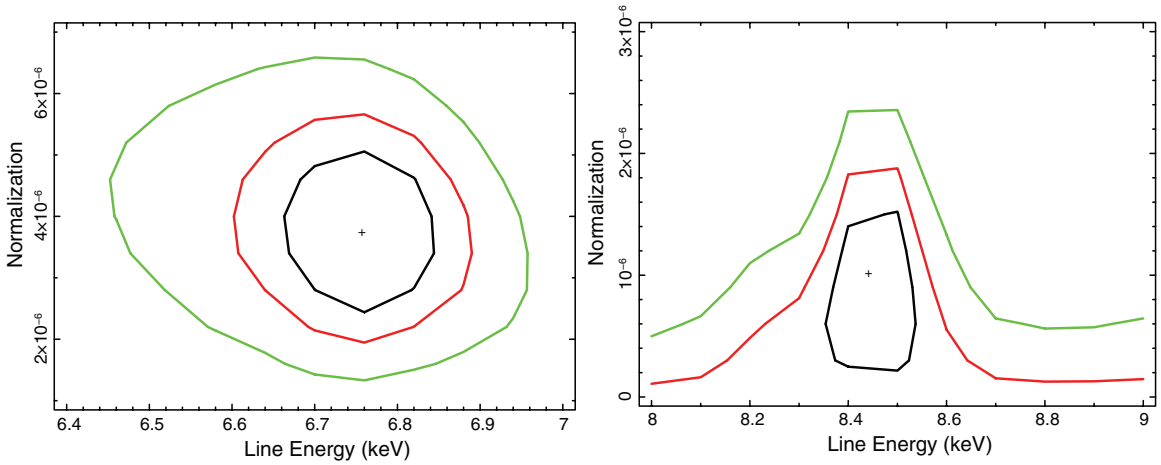

Figure 5. Confidence contours of the Fe 6.9 keV line (left panel) and the 8.1 keV line (right panel). The iron line is detected at a high significance level whereas detection of the 8.1 keV line is not significant above 1σ level.

(A color version of this figure is available in the online journal.)

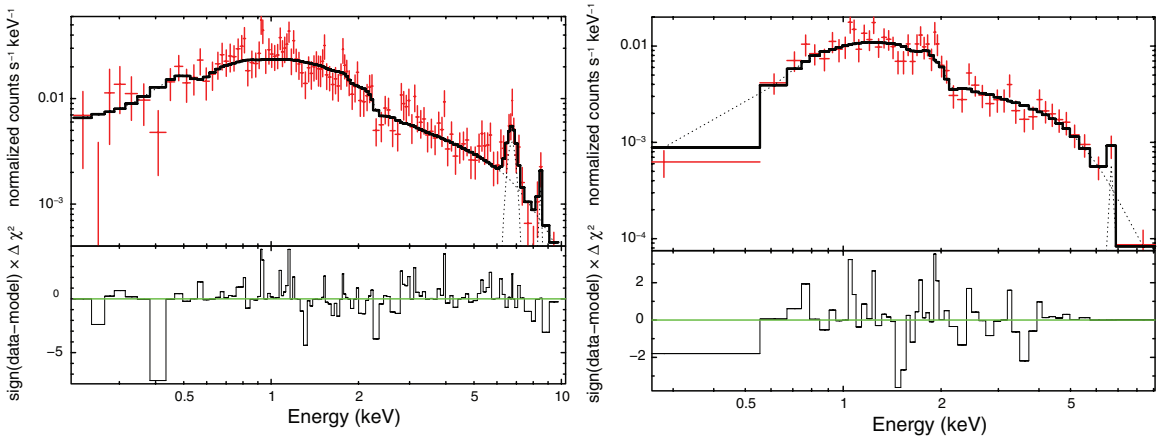

Figure 6. Left panel shows the *XMM-Newton* spectrum of SN 2006jd and the right panel shows the *Chandra* spectrum of SN 2006jd. Note that the 6.9 keV Fe line is detected in both spectra and has 10% of the total continuum flux (estimated from the *XMM-Newton* spectra).

(A color version of this figure is available in the online journal.)

Table 5
Spectral Model Fits to the *XMM-Newton* Spectrum

Model	χ^2/ν	$N_{\rm H}$	Param-1	Param-2	Abs. Flux	Unabs. Flux	Total Flux
PowerLaw	1.03(123)	$1.41^{+0.37}_{-0.30} \times 10^{21}$	$\Gamma = 1.31^{+0.15}_{-0.11}$	...	2.90×10^{-13}	3.33×10^{-13}	3.78×10^{-13}
+ Gaussian	...	...	$E = 6.76^{+0.10}_{-0.10}$	EW $= 1.02^{+0.16}_{-0.16}$	4.57×10^{-14}	4.58×10^{-14}	...
NEI	1.09(125)	$1.22^{+0.24}_{-0.18} \times 10^{21}$	$kT = 79.65^{+\cdots}_{-48.02}$	$\tau = 6.28^{+2.66}_{-1.55} \times 10^{11}$	3.25×10^{-13}	3.59×10^{-13}	3.59×10^{-13}
Mekal	1.12(126)	$1.38^{+0.22}_{-0.21} \times 10^{21}$	$kT = 36.77^{+\cdots}_{-20.18}$	...	3.09×10^{-13}	3.48×10^{-13}	3.48×10^{-13}
Bremsstrahlung	1.02(123)	$1.25^{+0.21}_{-0.23} \times 10^{21}$	$kT = 56.76^{+56.80}_{-28.83}$	...	2.91×10^{-13}	3.26×10^{-13}	3.64×10^{-13}
+ Gaussian	...	...	$E = 6.76^{+0.11}_{-0.10}$	EW $= 1.38^{+0.18}_{-0.13}$	3.75×10^{-14}	3.76×10^{-14}	...

Notes. Here, $N_{\rm H}$ is in $\rm cm^{-2}$, E and EW are in keV, τ in $\rm cm^{-3}$ s, and the fluxes are in $\rm erg\,cm^{-2}\,s^{-1}$. The fluxes mentioned are in the 0.2–10.0 keV energy range. The abs. and unabs. fluxes are of that particular component in the model, whereas the total flux is for the total unabsorbed flux of the model.

Boltzmann's constant, μ is the mean molecular weight, and m_p is the proton mass. The shock velocity is closer to expectations for the forward shock than the reverse shock wave at this age, although X-ray emission from young SNe is typically attributed to the reverse shock wave (Chevalier & Fransson 2003). A high-velocity reverse shock wave is possible if the SN runs into a dense medium which acts as a wall for the expanding SN gas; such a situation is observed in SN 1987A. However, this situation is expected to produce rising fluxes at radio and X-ray wavelengths followed by a turnover. The fluxes in SN 2006jd are observed to decline slowly from days 400 through 1700, so we consider a forward shock origin to be more likely.

We found that the temperature of the emitting region is higher than can be measured in the 0.2–10 keV bandpass of the X-ray detectors, so that a spectral luminosity L_ν is measured rather than a total X-ray luminosity. For bremsstrahlung emission we have $L_\nu \propto n^2 V/T^{1/2}$, where V is the emitting volume, so that $L_\nu \propto t^{2m(1-s)+1}$. If the observed $L_\nu \propto t^{-x}$, then $x = 0.24$ for the present case (Figure 7). We have $x = 2m(s-1) - 1$ or $s = 1+(1+x)/2m = 1+0.62/m$. Taking $m = 0.9$ gives $s = 1.7$.

Table 6
Spectral Model Fits to the *Chandra* Spectrum

Model	χ^2/ν	$N_{\rm H}$	Param-1	Param-2	Abs. Flux	Unabs. Flux	Total Flux
PowerLaw	0.90(48)	$1.83^{+0.61}_{-0.53} \times 10^{21}$	$\Gamma = 1.34^{+0.17}_{-0.16}$	...	2.82×10^{-13}	3.24×10^{-13}	3.44×10^{-13}
+ Gaussian	...	...	$E = 6.67^{+1.24}_{-0.21}$	EW $= 0.73^{+1.12}_{-...}$	1.98×10^{-14}	1.98×10^{-14}	...
NEI	0.83(50)	$1.59^{+0.46}_{-0.38} \times 10^{21}$	$kT = 35.93^{+...}_{-20.32}$	$\tau = 3.72^{+4.51}_{-0.80} \times 10^{11}$	3.02×10^{-13}	3.36×10^{-13}	3.36×10^{-13}
Mekal	0.82(51)	$1.80^{+0.39}_{-0.35} \times 10^{21}$	$kT = 20.67^{+35.71}_{-7.63}$	...	2.96×10^{-13}	3.36×10^{-13}	3.36×10^{-13}
Bremsstrahlung	0.91(48)	$1.61^{+0.47}_{-0.35} \times 10^{21}$	$kT = 41.61^{+...}_{-27.77}$	...	2.78×10^{-13}	3.13×10^{-13}	3.35×10^{-13}
+ Gaussian	...	...	$E = 6.72^{+0.74}_{-0.22}$	EW $= 0.83^{+0.35}_{-...}$	2.20×10^{-14}	2.20×10^{-14}	...

Notes. Here, $N_{\rm H}$ is in cm^{-2}, E and EW are in keV, τ in cm^{-3} s, and the fluxes are in erg cm^{-2} s^{-1}. The fluxes mentioned are in the 0.2–10.0 keV energy range. The abs. and unabs. fluxes are for that particular component in the model, whereas the total flux is for the total unabsorbed flux of the model.

Table 7
Unabsorbed 0.2–10 keV X-Ray Fluxes of SN 2006jd at Various Epochs

Date of Observation	Days since Explosion	Instrument	Flux (10^{-13} erg cm^{-2} s^{-1})	Luminosity (10^{41} erg s^{-1})
2007 Nov 16.73–22.84	403.2 ± 3.1	*Swift*-XRT	4.51 ± 0.73	3.37 ± 0.54
2007 Dec 18.01	431.5	*Swift*-XRT	4.28 ± 0.73	3.19 ± 0.54
2008 Jan 15.32	459.8	*Swift*-XRT	4.91 ± 0.79	3.67 ± 0.59
2008 Feb 20.18–21.32	496.2 ± 0.6	*Swift*-XRT	3.98 ± 0.66	2.97 ± 0.49
2008 Sep 09.02–11.02	698.5 ± 1.0	*Swift*-XRT	5.35 ± 0.73	4.00 ± 0.54
2009 Apr 07.20	907.7	*XMM* EPIC-PN	$3.63^{+0.33}_{-0.30}$	$2.70^{+0.25}_{-0.23}$
2009 Sep 10.12	1063.6	*Swift*-XRT	3.01 ± 0.60	2.25 ± 0.45
2009 Sep 14.00	1067.5	*Chandra* ACIS-S	$3.38^{+0.89}_{-0.93}$	$2.52^{+0.70}_{-0.66}$
2011 Mar 08.32–12.41	1609.8 ± 2.0	*Swift*-XRT	3.71 ± 0.60	2.77 ± 0.45

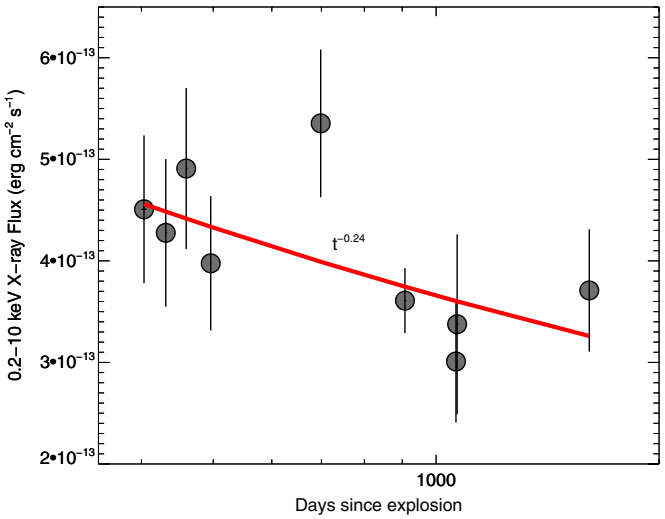

Figure 7. X-ray light curve of SN 2006jd. The light curve is best fit with a power law of index -0.24 ± 0.12.

(A color version of this figure is available in the online journal.)

The radio and X-ray observations thus give $s \approx 1.6$, which is similar to the value deduced for SN 2010jl from observations at a earlier epoch (Chandra et al. 2012). Using results from Fransson et al. (1996) for L_ν as in Chandra et al. (2012) the mass-loss rate $\dot{M}$, normalized to $R = 10^{15}$ cm, is $\dot{M}_{-3}/v_{w2} \approx 5 v_4^{0.6}$, where $\dot{M}_{-3} = \dot{M}/(10^{-3}\, M_\odot\ {\rm yr}^{-1})$, v_{w2} is the preshock wind velocity in units of 100 km s^{-1}, and v_4 is the average velocity in units of 10^4 km s^{-1} at 10^3 days. At 10^3 days, the preshock density is $2 \times 10^{-18}\, v_4^{-1}$ g cm^{-3}. The corresponding density in the shocked gas is $n_{\rm H} \sim 3 \times 10^6$ cm^{-3}.

The observed X-ray spectrum is well fit by a single temperature model, and there is no sign of emission from a reverse shock region. One possible reason for the lack of such emission is that the SN interaction has evolved to the point where the reverse shock wave has moved back to the center and has weakened. In the model described above, the mass swept up by the forward shock is $M_{sw} = \dot{M} R_s / v_w \simeq 3\, M_\odot$. If the ejecta mass is significantly smaller than this, the reverse shock region is expected to decline in luminosity. Another possibility is that the reverse shock is a cooling shock and the cool shell absorbs the radiation from the reverse shock region. In addition, when the reverse shock is radiative, the luminosity from the reverse shock region rises as ρ_w, while that from the forward shock region rises as ρ_w^2. In SN 1993J, a hot (80 keV) thermal X-ray spectrum was observed in the first few weeks and interpreted as emission from the forward shock region, with emission from the reverse shock absorbed by a cooling shell (Leising et al. 1994; Fransson et al. 1996). The conditions for radiative cooling at the reverse shock depend on the density profile of the ejecta, and there is a transition to nonradiative evolution at late times. At the high densities inferred for SN 2006jd, that transition can be delayed.

Here we have assumed that the hot gas is in thermal equilibrium. The time for the electrons and protons to come into equilibrium is $t_{ep} \sim 3$ yr for $kT = 50$ keV and $n_e = 10^6$ cm^{-3} (Spitzer 1962). At an age of 1000 days, the electrons and protons are thus close to equilibrium by Coulomb interactions and may be brought even closer to equilibrium by plasma instabilities. If equilibrium has not been obtained, the shock velocity is somewhat higher than what we have deduced here.

A robust result of fitting the X-ray spectrum is the hydrogen column density $N_{\rm H}$ to the source. Of the $N_{\rm H} = 1.3 \times 10^{21}$ cm^{-2} that is observed, 4.5×10^{20} cm^{-2} can be attributed to the Galaxy, so there is 8.5×10^{20} cm^{-2} left for the SN host galaxy interstellar medium and the SN CSM. This column density estimate assumes that the absorbing medium has solar abundances, and is

cool and not highly ionized. In the model for the X-ray emission discussed above, the expected column density in the unshocked CSM is 4×10^{22} cm^{-2}, a factor of 50 larger than that inferred from the observations. A possible reason is that the CSM is fully ionized by the X-ray radiation. However, the ionization parameter for this case is $\xi = L/nr^2 = 50$, which indicates that there may be some ionization of CNO elements, but not full ionization of the gas (Verner & Ferland 1996). To check on this result, we ran the CLOUDY code (Ferland et al. 1998) for the parameters discussed above. As expected, we found some ionization of CNO elements, but little change in the absorption of the X-ray spectrum.

The temperature of the CSM is relevant to the absorption of the radio emission from the shocked region. In the CLOUDY simulation, we found an electron temperature somewhat less than 10^5 K, which is consistent with the ionization parameter. Using Equation (20) of Chevalier & Fransson (2003) and the circumstellar parameters derived from the X-ray luminosity, the wind optical depth at 5 GHz on day 1000 is $\tau_{\rm ff} = 2.4 T_{e5}^{-3/2}$, where T_{e5} is the electron temperature in units of 10^5 K. The optical depth is thus consistent with that indicated by the observations (Figure 2). The radio emission is expected to be from the high-temperature X-ray emitting region, and we have seen that the absorbing column to the X-ray emitting region is relatively small. Assuming that the inner radius is like that found for the X-rays and scaling to the lower column density (upper limit) leads to $\tau_{\rm ff} = 8 \times 10^{-4} T_{e5}^{-3/2}$ at 5 GHz on day 1000. The high ionization parameter in this case gives $T_{e5} > 1$, so the FFA along the line of sight to the X-ray emission fails to produce the observed radio absorption. This is consistent with our analysis of the radio emission, which showed that external FFA does not lead to good model fits to the data.

Another robust result from the X-ray spectrum is the finding of an Fe emission line feature centered at 6.9 keV rest energy (using $z = 0.0186$), with an equivalent width of 1.4 keV. The collisional equilibrium model that fits the continuum emission has a weak Fe line (0.1 keV equivalent width) at an energy of 6.9 keV. The model line is much weaker than that observed. We considered the possibility of ionization nonequilibrium by using the nonequilibrium model in XSPEC. The model depends on the postshock temperature, which was fit with 60 keV, and the ionization time $\tau_i = nt$, which we varied for various fits. We found that for $\tau_i = 6 \times 10^{11}$ cm^{-3} s the model provided a good fit to the data, with $\chi^2/{\rm dof} = 1.03$; both the equivalent width and the line energy were well fit. However, considering the age of 1000 days, this implies the density to be $\sim 7 \times 10^3$ cm^{-3} (Section 2.2), much less than the density in the hot gas, $n_{\rm H} \sim 3 \times 10^6 v_4^{-1}$ cm^{-3}, needed to produce the X-ray luminosity. Raising τ_i in the nonequilibrium model, we found that by $\tau_i = 5 \times 10^{12}$ cm^{-3} s, the line was essentially the same as in equilibrium, showing that any density close to that needed for the X-ray luminosity fails to produce the Fe line. The nonequilibrium model in XSPEC assumes a Sedov blast wave model for the hydrodynamics, which is different from the situation studied here, but we do not expect a significant change in the results.

The equivalent width of Kα line thus exceeds values predicted by ionization equilibrium models. A scenario that might resolve the issue involves the presence of the cool dense shell that is formed from cooled gas at the reverse shock wave. The shell is subject to the Rayleigh–Taylor instability so that the forward postshock zone turns into a two-phase mixture composed of rarefied hot and dense cool gas (Chevalier & Blondin 1995; Blondin & Ellison 2001). The observed X-ray continuum with a weak Kα line presumably arises from the hot component. The two-phase mixture, however, could enhance the production rate of Kα photons because of the efficient recombination of hot Fe^{+26} ions penetrating the cool phase with low-temperature electrons. This can be illustrated as follows. The total recombination rate in the kth phase (k is "cool" or "hot") is $R_k \propto p_k \alpha_k n_{e,k}$, where p_k is the probability for the fast Fe^{+26} ion to get into kth phase, $\alpha_k \propto T_{e,k}^{-\eta}$ is the recombination coefficient, and $n_{e,k}$ is the electron number density. Assuming p_k to be proportional to the volume filling factor of the corresponding phase (which requires strong mixing), we find that the ratio of recombination rates of fast Fe^{+26} ions in the cool and hot phases is $R_{c,h} = (M_c/M_h)(T_h/T_{c,{\rm eff}})^\eta$, where M_k is the mass of the corresponding phase and $T_{c,{\rm eff}} = \max[T_c, T_h(m_e/56\,m_p)]$ is the effective temperature that determines the relative velocity of cool electrons and hot Fe^{+26} ions. Adopting $T_h = 50$ keV, $T_c = 0.001$ keV, and $\eta = 0.7$, we obtain $R_{c,h} \approx 2 \times 10^3 (M_c/M_h)$, which suggests that even a low-mass cool phase $M_c \sim 10^{-3} M_h$ could dominate the Kα line emission. Keeping in mind that the cool phase does not contribute to the X-ray continuum at 6.9 keV, we thus conclude that the proposed mechanism could significantly increase the equivalent width of the Kα line compared to a single-phase hot plasma. However, it is not clear whether the required penetration of Fe ions into the cold gas could take place. A magnetic field could inhibit the motion of Fe ions. Also, if magnetic field effects are small, there is likely to be an intermediate-temperature zone between the hot and cool phases, and the Fe^{+26} ions could recombine there. Our main point is that the cool gas presents some possibilities for Fe line emission. We argued in Section 3.1 that the absorption of the radio emission may also be related cool gas that is mixed into the shocked, hot gas.

4. DISCUSSION AND CONCLUSIONS

The basic interpretation of the X-ray and radio data in terms of standard spherical models led to inconsistencies. One is that the column density of matter to the X-ray emission is about a factor 50 smaller than that needed to produce the X-ray luminosity. Since the absorption column is $\propto \rho_w$ and the X-ray luminosity to ρ_w^2, one possibility is that the luminosity is enhanced by clumpiness of the gas. However, clumpiness would raise the shock velocity needed to produce a particular X-ray temperature and the temperature is already close to that expected behind the forward shock, so this solution does not seem feasible. The situation, however, may be different in the case that the circumstellar clouds interact primarily with the cool dense shell. Then the cloud shock velocity is large enough to account for the high temperature derived from the observed X-ray spectrum. The straightforward explanation is then that there is a global asymmetry in the distribution of the circumstellar gas that allows a low column density in one direction, while dense interaction is taking place over much of the rest of the solid angle (as viewed from the SN). Chugai & Danziger (1994) had suggested a scenario with equatorial mass loss to explain the presence of fast- and intermediate-velocity shock fronts in the Type IIn SN 1988Z. Polarization observations of SNe IIn have shown evidence for large-scale asymmetry, e.g., SN 1997eg (Hoffman et al. 2008), SN 1998S (Leonard et al. 2000), and SN 2010jl (Patat et al. 2011).

In this view, the column density to the radio emission would be small, as for the X-ray emission, because they are both from the same region. The external FFA model for the radio absorption thus fails, and an absorption mechanism internal to the emission is indicated. We have argued that thermal absorption internal to the emitting region is a plausible mechanism, as has previously been proposed for other SNe IIn (Weiler et al. 1990).

There is evidence that the X-ray properties we have found for SN 2006jd are not unusual for a Type IIn event. *Chandra* observations of SN 2001em and SN 2005dk have shown hard emission (Pooley & Lewin 2004; Pooley et al. 2007), implying a high temperature. In the case of SN 2001em, the column density is lower than expected from the X-ray luminosity (Chugai & Chevalier 2006), as in SN 2006jd. Another point of comparison is the Type IIn SN 2010jl, which had an unabsorbed 0.2–10 keV luminosity of $\sim 7 \times 10^{41}$ erg s^{-1} at ages of 2 months and 1 yr (Chandra et al. 2012). Although the X-ray luminosity is just a factor of two higher than that of SN 2006jd, the absorbing column, 10^{24} cm^{-2} at 2 months and 3×10^{23} cm^{-2} at 1 yr, is much higher. In this case, the observed column is roughly consistent with that needed to produce the X-ray luminosity. The implication is that the observed line of sight passes through the dense preshock gas for SN 2010jl, but not for SN 2006jd.

In this paper we have treated the radio and X-ray properties of SN 2006jd. A more comprehensive study would include observations at other wavelengths. SN 2006jd was detected as an infrared source at an age $\sim$1150 days (Fox et al. 2011). Its luminosity was $\sim 10^{42}$ erg s^{-1} which is larger than the X-ray luminosity observed at this time. If the interpretation of this emission as from circumstellar dust heated by shock emission is correct (Fox et al. 2011), it appears that some of the X-ray emission from the shocked region is shielded from the observer. An infrared/X-ray ratio >1 has also been observed in other SNe IIn (Gerardy et al. 2002).

Our observations at both radio and X-ray wavelengths imply that the circumstellar density profile ($\rho \propto r^{-2}$) is flatter than the $s = 2$ case that would be expected for a steady wind. We find $s = (1.5–1.6)$; deviation from the steady case is plausible for a SN IIn because the mass loss may be due to an eruptive event. In addition, the optical luminosity evolution of SN 2006jd shows a second peak at $\sim$500 days (Stritzinger et al. 2012) that is indicative of a nonstandard density distribution.

P.C. and R.C. are grateful to Craig Sarazin for discussions on X-ray emission and analysis. The National Radio Astronomy Observatory is a facility of the National Science Foundation operated under cooperative agreement by Associated Universities, Inc. P.C. is supported by her NSERC Discovery grants. R.C. and C.I. acknowledge support from NASA grants NNX09AH58G (*XMM*) and GO9–0079X (*Chandra*), and NSF grant AST-0807727.

Facilities: CXO, XMM, Swift, VLA, EVLA, GMRT

REFERENCES

Blondin, J. M., & Ellison, D. C. 2001, ApJ, 560, 244
Blondin, S., Modjaz, M., Kirshner, R., et al. 2006, CBET, 679, 1
Bregman, J. N., & Pildis, R. A. 1992, ApJ, 398, L107
Bregman, J. N., & Pildis, R. A. 1994, ApJ, 420, 570
Chandra, P., Chevalier, R. A., Irwin, C. M., et al. 2012, ApJ, 750, L2
Chandra, P., & Soderberg, A. 2007, ATel, 1297, 1
Chevalier, R., & Blondin, J. M. 1995, ApJ, 444, 312
Chevalier, R. A. 1982, ApJ, 259, 302
Chevalier, R. A. 1998, ApJ, 499, 810
Chevalier, R. A., & Fransson, C. 2003, in Supernovae and Gamma-Ray Bursters, ed. K. Weiler (Lecture Notes in Physics, Vol. 598; Berlin: Springer), 171
Chugai, N. N. 1990, Sov. Astron. Lett., 16, 457
Chugai, N. N., & Chevalier, R. A. 2006, ApJ, 641, 1051
Chugai, N. N., & Danziger, I. J. 1994, MNRAS, 268, 173
Fabian, A. C., & Terlevich, R. 1996, MNRAS, 280, L5
Fassia, A., Meikle, W. P. S., Chugai, N., et al. 2001, MNRAS, 325, 907
Ferland, G. J., Korista, K. T., Verner, D. A., et al. 1998, PASP, 110, 761
Filippenko, A. V. 1997, ARA&A, 35, 309
Fox, O. D., Chevalier, R. A., Skrutskie, M. F., et al. 2011, ApJ, 741, 7
Fransson, C., & Björnsson, C.-I. 1998, ApJ, 509, 861
Fransson, C., Lundqvist, P., & Chevalier, R. A. 1996, ApJ, 461, 993
Gal-Yam, A., & Leonard, D. C. 2009, Nature, 458, 865
Gerardy, C. L., Fesen, R. A., Nomoto, K., et al. 2002, ApJ, 575, 1007
Hoffman, J. L., Leonard, D. C., Chornock, R., et al. 2008, ApJ, 688, 1186
Immler, S., Brown, P. J., Filippenko, A. V., & Pooley, D. 2007, ATel, 1290, 1
Leising, M. D., Kurfess, J. D., Clayton, D. D., et al. 1994, ApJ, 431, L95
Leonard, D. C., Filippenko, A. V., Barth, A. J., & Matheson, T. 2000, ApJ, 536, 239
Li, W., Leaman, J., Chornock, R., et al. 2011, MNRAS, 412, 1441
Patat, F., Taubenberger, S., Benetti, S., Pastorello, A., & Harutyunyan, A. 2011, A&A, 527, L6
Pooley, D., Immler, S., & Filippenko, A. V. 2007, ATel, 1023, 1
Pooley, D., & Lewin, W. H. G. 2004, IAU Circ., 8323, 2
Prasad, R. R., & Li, W. 2006, CBET, 673, 1
Schlegel, E. M. 1990, MNRAS, 244, 269
Schlegel, E. M., & Petre, R. 2006, ApJ, 646, 378
Smartt, S. J. 2009, ARA&A, 47, 63
Spitzer, L. 1962, Physics of Fully Ionized Gases (2nd ed.; New York: Interscience)
Stritzinger, M., Taddia, F., Fransson, C., et al. 2012, arXiv:1206.5575
Temple, R. F., Raychaudhury, S., & Stevens, I. R. 2005, MNRAS, 362, 581
van Dyk, S. D., Weiler, K. W., Sramek, R. A., et al. 1996, AJ, 111, 1271
van Dyk, S. D., Weiler, K. W., Sramek, R. A., & Panagia, N. 1993, ApJ, 419, L69
Verner, D. A., & Ferland, G. J. 1996, ApJS, 103, 467
Weiler, K. W., Panagia, N., Montes, M. J., & Sramek, R. A. 2002, ARA&A, 40, 387
Weiler, K. W., Panagia, N., & Sramek, R. A. 1990, ApJ, 364, 611
Williams, C. L., Panagia, N., Van Dyk, S. D., et al. 2002, ApJ, 581, 396